

Synthesis, Crystal Structure, and Molecular Modeling of a Layered Manganese(II) Phosphate: $\text{Mn}_3(\text{PO}_4)_4 \cdot 2(\text{H}_3\text{NCH}_2\text{CH}_2)_3\text{N} \cdot 6(\text{H}_2\text{O})$

Steven G. Thoma,^{*,†} François Bonhomme,[‡] and Randall T. Cygan[‡]

Organic Materials Department and Geochemistry Department, Sandia National Laboratories, P.O. Box 5800, MS 1421, Albuquerque, New Mexico 87185-1421

Received September 11, 2003. Revised Manuscript Received March 19, 2004

A novel layered manganese(II) phosphate, $\text{Mn}_3(\text{PO}_4)_4 \cdot 2(\text{H}_3\text{NCH}_2\text{CH}_2)_3\text{N} \cdot 6(\text{H}_2\text{O})$, has been synthesized solvothermally using tris(2-aminoethyl)amine (TREN) as a template. The structure was solved ab initio using X-ray powder diffraction data and confirmed by molecular modeling. The compound was further characterized by SEM, IR spectroscopy, photoluminescence, and elemental and thermal analysis. The compound crystallizes in the trigonal space group $P\bar{3}c1$ with $a = 8.8706(4)$ Å, $c = 26.158(2)$ Å, and $V = 1782.6(2)$ Å³. The structure consists of layers of corner sharing Mn(II)O₄ and PO₄ tetrahedra forming infinite $[\text{Mn}_3(\text{PO}_4)_4]^{6-}$ macroanions with 4.6 net topology, sandwiched by layers of TREN and water molecules. The protonated TREN molecules provide charge balancing for the inorganic sheets; the interlayer stability is accomplished mainly by a network of hydrogen bonds between water molecules and the inorganic macroanions. This hybrid organic/inorganic layered material can be reversibly dehydrated.

Introduction

The design of new microporous phases is a rapidly expanding field, motivated largely by their potential application as catalysts, ion exchangers, and molecular sieves. Organically templated metal–phosphates, in particular, have greatly extended this family that was historically composed almost entirely of aluminosilicates.¹ Although many alumino-, gallo-, and zinc-phosphates are known, and a great number of microporous manganese oxide phases exist,^{2,3} few microporous manganese phosphate phases have been synthesized to date. In fact, virtually no porous manganese phosphate phases had been characterized prior to 1999.¹

With the exception of $\text{Na}_2\text{Mn}_2\text{O}(\text{PO}_4)_2 \cdot \text{H}_2\text{O}^4$ and $\text{NH}_4\text{-Mn}_4(\text{PO}_4)_3$,⁵ every open framework pure manganese phosphate (or phosphite) compound synthesized to date required the use of an organic template as structure directing agent, as had been suggested by Rajic et al.⁶ Most of these compounds are layered^{4,7–11} whereas structurally characterized phases with a 3-dimensional network contain pillaring oxalate units.^{12,13}

The most prolific organic template used in the synthesis of uncondensed manganese phosphate (or phosphite) compounds has been ethylenediamine^{6,7,10,11,13,14} although piperazine⁸ and $>\text{C}_2$ alkyldiammonium compounds^{6,9,12} were also used successfully. Tris(2-aminoethyl)amine (TREN) has not been reported as a templating agent for manganese phosphate synthesis though it has been used for open framework aluminophosphate,¹⁵ fluoroaluminophosphate,¹⁶ fluorogallophosphate,¹⁷ layered aluminophosphates,^{18,19} and a layered fluorogallophosphate.²⁰ In this paper, we report the synthesis and characterization of a novel layered manganese(II) phosphate compound templated by TREN, $\text{Mn}_3(\text{PO}_4)_4 \cdot 2(\text{H}_3\text{NCH}_2\text{CH}_2)_3\text{N} \cdot 6(\text{H}_2\text{O})$.

Experimental Section

Synthesis. Typically, 0.46 g of manganese carbonate (Aldrich, 99.9+%) was dissolved in a solution of 3.00 g of deionized water and 0.60 g of phosphoric acid (Fisher Scientific, 85%).

* Corresponding author. Phone: (505) 844-0612. E-mail: sgthoma@sandia.gov.

[†] Organic Materials Department.

[‡] Geochemistry Department.

(1) Cheetham, A. K.; Ferey, G.; Loiseau, T. *Angew. Chem., Int. Ed.* **1999**, *38*, 3269.

(2) Feng, Q.; Hirofumi, K.; Ooi, K. *J. Mater. Chem.* **1999**, *9*, 319.

(3) Xia, G.-G.; Tong, W.; Tolentino, E. N.; Duan, N. G.; Brock, S. L.; Wang, J. Y.; Suib, S. L.; Ressler, T. *Chem. Mater.* **2001**, *13*, 1585.

(4) Tong, W.; Xia, G.-G.; Tian, Z.-R.; Liu, J.; Cai, J.; Suib, S. L.; Hanson, J. C. *Chem. Mater.* **2002**, *14*, 615.

(5) Neeraj, S.; Noy, M. L.; Cheetham, A. K. *Solid State Sci.* **2002**, *4*, 397.

(6) Rajic, N.; Ristic, A.; Kaucic, V. *Zeolites* **1996**, *17*, 304.

(7) Escobal, J.; Pizarro, J. L.; Mesa, J. L.; Lezama, L.; Olazcuaga, R.; Arriortua, M. I.; Rojo, T. *Chem. Mater.* **2000**, *12*, 376.

(8) Kongshaug, K. O.; Fjellvag, H.; Lillerud, K. F. *J. Solid State Chem.* **2001**, *156*, 32.

(9) Fernandez, S.; Pizarro, J. L.; Mesa, J. L.; Lezama, L.; Arriortua, M. I.; Olazcuaga, R.; Rojo, T. *Inorg. Chem.* **2001**, *40*, 3476.

(10) Fernandez, S.; Mesa, J. L.; Pizarro, J. L.; Lezama, L.; Arriortua, M. I.; Olazcuaga, R.; Rojo, T. *Chem. Mater.* **2000**, *12*, 2092.

(11) Chippindale, A. M.; Gaslain, F. O. M.; Cowley, A. R.; Powell, A. V. *J. Mater. Chem.* **2001**, *11*, 3172.

(12) Lethbridge, Z. A. D.; Hillier, A. D.; Cywinski, R.; Lightfoot, P. *J. Chem. Soc., Dalton Trans.* **2000**, *11*, 1595.

(13) Lethbridge, Z. A. D.; Tiwary, S. K.; Harrison, A.; Lightfoot, P. *J. Chem. Soc., Dalton Trans.* **2001**, *12*, 1904.

(14) Hsu, K. F.; Wang, S. L. *Inorg. Chem.* **2000**, *39*, 1773.

(15) Xu, Y.-H.; Zhang, B.-G.; Chen, X.-F.; Liu, S.-H.; Duan, C.-Y.; You, X.-Z. *J. Solid State Chem.* **1999**, *145*, 220.

(16) Simon, N.; Loiseau, T.; Ferey, G. *Solid State Sci.* **1999**, *1*, 339.

(17) Weigel, S. J.; Weston, S. C.; Cheetham, A. K.; Stucky, G. D. *Chem. Mater.* **1997**, *9*, 1293.

(18) Simon, N.; Loiseau, T.; Ferey, G. *J. Mater. Chem.* **1999**, *9*, 585.

(19) Simon, N.; Loiseau, T.; Ferey, G. *Solid State Sci.* **2000**, *2*, 389.

(20) Serpaggi, F.; Loiseau, T.; Riou, D.; Ferey, G. *Eur. J. Solid State Inorg. Chem.* **1994**, *31*, 595.

Pyridine (5.00 g) (Aldrich, 99+%) was added slowly with vigorous stirring, followed by 0.58 g of TREN (Aldrich, 96%), resulting in a thick brown gel. The number of moles in the precursor mixture were 4.0 mmol of manganese carbonate/5.2 mmol of phosphoric acid/4.0 mmol of TREN/63.2 mmol of pyridine/171.6 mmol of water (from all sources), resulting in a molar ratio of 1.0 Mn/1.3 P/1.0 TREN/15.8 pyridine/42.9 water. This mixture was then transferred to a 23 mL Teflon lined steel autoclave and heated at 170 °C for 5 days. After cooling to room temperature, the sample was vacuum filtered, washed with deionized water and acetone, and oven dried in air at 50 °C.

Characterization. SEM images were recorded using a JEOL JSM-6300V scanning electron microscope (SEM) and Iridium (IXRF Systems) software. Thermal analysis was performed using a TA Instruments SDT 2960 simultaneous thermogravimetric analyzer–differential thermal analyzer (TGA–DTA). The density was determined using a Micromeritics AccuPyc 1330 helium pycnometer. Elemental analysis was performed by Galbraith, Inc. (Knoxville, TN), using inductively coupled plasma spectroscopy for manganese and phosphorus, and combustion methods for carbon, hydrogen, and nitrogen. X-ray powder diffraction was performed with a Siemens D-500 and a Bruker D8-Advance diffractometer in Bragg–Brentano geometry with Ni-filtered Cu K α radiation; preferred orientation was minimized by back loading of the sample. Infrared spectra were recorded within the range 370–4000 cm⁻¹ on a Perkin-Elmer Spectrum GX FTIR spectrometer using the KBr pellet method. Photoluminescence measurements were made at room temperature using a SPEX Fluorlog II. pH measurements were made using a Corning pH meter and electrode.

Structure Determination. Since no suitable single crystal was obtained, an ab initio structure determination from powder diffraction data was carried out. The positions of the first 35 peaks were refined with the program XFIT²¹ using a split Pearson VII function for the more asymmetric low angle peaks and a pseudo-Voigt function for the peaks above 15°. The peak positions were calibrated using silicon SRM640 and silver behenate²² as external standards. A sharp diffraction peak at 2 θ = 10.0° belonging to a minor lamellar impurity phase (likely NH₄MnPO₄·H₂O²³) was excluded from the peak list. The pattern was then indexed with good figures of merit²⁴ (M_{20} = 43, F_{20} = 69) by the program TREOR90²⁵ with a hexagonal cell of approximate cell parameters a = 8.87 Å and c = 26.16 Å with V = 1783 Å³. The refined lattice constants obtained using the program LATCON²⁶ are given Table 1. The reflection conditions ($h0l$ and $00l$ with l even) correspond to the space groups $P6_3cm$, $P6_3c2$, or $P6_3/mcm$. A whole pattern profile refinement by the Le Bail method,²⁷ using the program FULLPROF98,²⁸ confirmed the adequacy of this cell and systematic absences. In contrast, all attempts at solving the structure with a hexagonal symmetry failed. As the metric of the cell was apparently well established, we then carried out the structure determination with a trigonal symmetry. The only two space groups consistent with the observed extinction laws were $P3c1$ and $P\bar{3}c1$.

The structure was eventually solved successfully in $P\bar{3}c1$ using the EXPO²⁹ package, which combines an integrated

Table 1. Crystal Data and Structure Refinement Parameters

compound	Mn ₃ (PO ₄) ₄ ·2(N ₄ C ₆ H ₂₁)·6(H ₂ O)
chemical formula	Mn ₃ P ₄ O ₂₂ N ₈ C ₁₂ H ₅₄
formula weight	951.3 g/mol
crystal system	trigonal
space group	$P\bar{3}c1$ (No. 165)
unit cell dimensions	a = 8.8706(4) Å c = 26.158(2) Å
Volume	1782.6(2) Å ³
Z	2
D (measured)	1.80(1) g/cm ³
D (calcd)	1.77 g/cm ³
$F(000)$	986
T	298(2) K
wavelength	Cu K $\alpha_{1,2}$
2 θ range	2.5–80.0°
step size 2 θ	0.04°
time per step	60 s
min fwhm	0.14°
no. free params ^a	40
no. structural params ^a	29
no. indep reflns	370
no. soft constraints	3 distances and 3 angles constrained: N–C = 1.48(1) Å (2 \times); C–C = 1.51(1) Å (1 \times) C–N–C = 112.0(1)° (1 \times) N–C–C = 112.0(1)° (2 \times)
final R indices (background subtracted)	R_p = 8.45%; R_{wp} = 10.60% R_{exp} = 2.96%; χ^2 = 12.93 R_{Bragg} = 2.62%

^a 24 positional parameters and 5 isotropic atomic displacement parameters. 11 profile parameters: scale factor; 2 cell parameters; sample displacement correction; 2 variable pseudo-Voigt parameters; U , V , W ; 2 asymmetry parameters.

intensities extraction routine (EXTRA³⁰) and a direct method program (SIRPOW³¹) optimized for powder diffraction data. The imperfect crystallinity of the compound led to peak broadening ($fwhm_{min}$ = 0.14°) and hence very severe nonsystematic overlap at high angles. It was therefore necessary to try different angular limits for the pattern decomposition in order to obtain a sufficient number of still meaningful intensities. Furthermore, the systematic overlap of nonequivalent reflections for this space group further degraded the reliability of the extracted equipartitioned intensities.

With such a low quality data set, the prior knowledge of the phase composition is of paramount importance for a successful structure determination. The elemental chemical analysis gave the atomic ratio Mn/P = 0.76; the organic fraction had the composition C₆N_{3.96}H_{28.11}, showing that the TREN molecule was very likely intact and the phosphorus to TREN ratio was 1.97. Thermogravimetric analysis showed a weight loss of 11.2 wt % below 200 °C that can be attributed to water loss. Those analyses and the measured density of 1.80(1) g/cm³ suggested the idealized composition of Mn₃(PO₄)₄·2(N₄C₆H₂₁)·6(H₂O), with Z = 2.

The best E-map obtained from this inherently limited data set was very noisy but revealed the location of the manganese site and of one of the two phosphorus sites; the third and fourth ranking peaks in the list turned out, however, to be spurious. The overall 2D character of the structure suggested by the crystallites morphology was nevertheless already evidenced.

By treating the PO₄ tetrahedron as a rigid body, we could build a reasonable partial model that was gradually completed by alternating cycles of refinement and difference Fourier map interpretation. The second independent phosphorus atom was immediately located on a site with 3-fold symmetry, which

(21) Cheary R. W.; Coelho, A. A. *J. Appl. Crystallogr.* **1992**, *25*, 109.

(22) Blanton, T. N.; Barnes, C. L.; Lelental, M. *J. Appl. Crystallogr.* **2000**, *33*, 172.

(23) Carling, S. G.; Day, P.; Visser, D. *J. Inorg. Chem.* **1995**, *34*, 3917.

(24) de Wolff, P. M. *J. Appl. Crystallogr.* **1972**, *5*, 243.

(25) Werner, P. E.; Eriksson, L.; Westdahl, M. *J. Appl. Crystallogr.* **1985**, *18*, 367.

(26) Schwartzbach, D. [LATCON] *Xtal3.7 System*; Hall, S. R., du Boulay, D. J., Olthof-Hazekamp, R., Eds.; University of Western Australia, 2000.

(27) Le Bail, A.; Duroy, H.; Fourquet, J. *Mater. Res. Bull.* **1988**, *23*, 447.

(28) Rodriguez-Carvajal, J. A. In *Collected Abstracts of Powder Diffraction Meeting*; Toulouse, France, 1990; 127.

(29) Altomare, A.; Burla, M. C.; Camalli, M.; Carrozzini, B.; Cascarano, G. L.; Giacovazzo, C.; Guagliardi, A.; Moliterni, A. G. G.; Polidori, G.; Rizzi, R. *J. Appl. Crystallogr.* **1999**, *32*, 339.

(30) Altomare, A.; Burla, M. C.; Cascarano, G. L.; Giacovazzo, C.; Guagliardi, A.; Moliterni, A. G. G.; Polidori, G. *J. Appl. Crystallogr.* **1995**, *28*, 842.

(31) Altomare, A.; Cascarano, G. L.; Giacovazzo, C.; Guagliardi, A.; Burla, M. C.; Polidori, G.; Camalli, M. *J. Appl. Crystallogr.* **1994**, *27*, 435.

Table 2. Atomic Coordinates from Rietveld Refinement (Bold) and Molecular Modeling (Italics) for Non-Hydrogen Atoms for $\text{Mn}_3(\text{PO}_4)_4 \cdot 2(\text{N}_4\text{C}_6\text{H}_{21}) \cdot 6(\text{H}_2\text{O})^a$

atom-site	x	y	z
Mn-6f	0.7415(5) <i>0.7363</i>	0 <i>0</i>	$\frac{1}{4}$ $\frac{1}{4}$
P1-4d	$\frac{1}{3}$ <i>$\frac{1}{3}$</i>	$\frac{2}{3}$ <i>$\frac{2}{3}$</i>	0.2373(4) <i>0.2436</i>
P2-4c	0 <i>0</i>	0 <i>0</i>	0.1681(3) <i>0.1838</i>
O1-4d	$\frac{1}{3}$ <i>$\frac{1}{3}$</i>	$\frac{2}{3}$ <i>$\frac{2}{3}$</i>	0.2957(6) <i>0.2947</i>
O2-12g	0.304(1) <i>0.2992</i>	0.491(1) <i>0.4892</i>	0.2231(4) <i>0.2282</i>
O3-12g	0.184(1) <i>0.1859</i>	0.094(1) <i>0.0905</i>	0.1899(3) <i>0.2010</i>
O4-4c	0 <i>0</i>	0 <i>0</i>	0.1082(6) <i>0.1323</i>
Ow-12g	0.149(1) <i>0.1348</i>	0.252(1) <i>0.2668</i>	0.0359(3) <i>0.0413</i>
N1-4d	$\frac{2}{3}$ <i>$\frac{2}{3}$</i>	$\frac{1}{3}$ <i>$\frac{1}{3}$</i>	0.0832(7) <i>0.0805</i>
N2-12g	0.440(2) <i>0.4216</i>	0.022(2) <i>0.0168</i>	0.1517(3) <i>0.1368</i>
C1-12g	0.515(2) <i>0.5407</i>	0.163(1) <i>0.1585</i>	0.0673(4) <i>0.0654</i>
C2-12g	0.495(2) <i>0.5269</i>	0.010(2) <i>0.0246</i>	0.0990(3) <i>0.0989</i>

^a Isotropic atomic displacement parameters: $B(\text{Mn}) = 2.8(1) \text{ \AA}^2$; $B(\text{P}) = 2.9(1) \text{ \AA}^2$; $B(\text{O}) = 3.1(2) \text{ \AA}^2$; $B(\text{Ow}) = 3.1(3) \text{ \AA}^2$; $B(\text{C}) = B(\text{N}) = 3.5(2) \text{ \AA}^2$.

allowed a rapid completion of the inorganic part of the structure. The oxygen environment around the Mn site turned out unexpectedly to be tetrahedral.

Assuming that the template molecules were ordered and undistorted, the central nitrogen atom of the TREN molecule was placed on a position with 3-fold axis site symmetry. Difference Fourier maps revealed gradually the position of the two remaining carbon atoms and of the terminal nitrogen. The TREN molecule was refined from the start using bond distance and angle constraints corresponding to typical values encountered in other TREN-templated metal phosphates.^{18–20} The template molecules are assumed to be triply protonated for charge balancing reasons, and their hydrogen positions were geometrically calculated using WinCrystals2001.³² These seven hydrogen sites were included in the final stages of the refinement and kept fixed at their idealized positions. Finally, the residual electron density corresponding to the missing water molecules was located on a general position between the hybrid layers.

The summary of crystallographic data, including the values of the geometrical constraints for the TREN molecule, is given Table 1. Non-hydrogen atom coordinates are presented Table 2, and selected bond lengths and bond angles are given in Tables 3 and 4, respectively. No evidence of an increase in symmetry from trigonal to hexagonal was observed in later analysis (option ADDSYM in PLATON³³). The constraints initially applied to the inorganic layer (semirigid PO_4 tetrahedra with $\text{P}-\text{O} = 1.56(1) \text{ \AA}$ and $\text{O}-\text{P}-\text{O} = 109(1)^\circ$) were fully relaxed at the end of the refinement process, and this did not lead to significant changes in bond distances and angles nor in an improvement of the agreement factors. The refinement eventually converged to a satisfactory agreement factor $R_{\text{Bragg}} = 2.63\%$. The observed and difference Rietveld plots are given in Figure 1.

Molecular Modeling. To both validate the structure determination obtained from the analysis of the X-ray powder

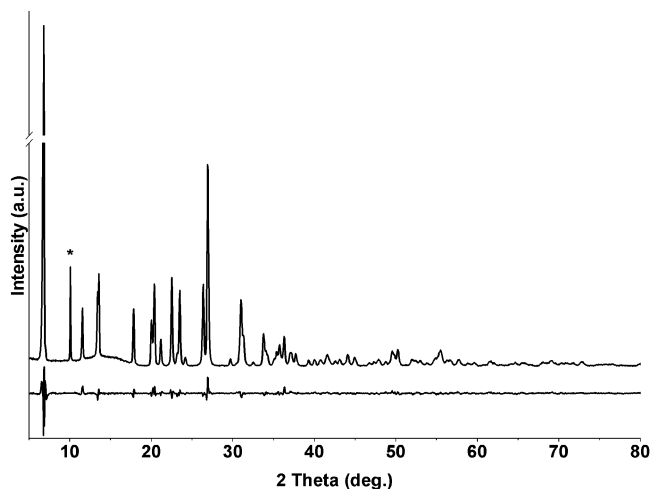


Figure 1. Observed and difference Rietveld plots for $\text{Mn}_3(\text{PO}_4)_4 \cdot 2(\text{N}_4\text{C}_6\text{H}_{21}) \cdot 6(\text{H}_2\text{O})$. Asterisk indicates impurity peak from $\text{NH}_4\text{MnPO}_4 \cdot \text{H}_2\text{O}$.²³

Table 3. Selected Bond Lengths [Å] for $\text{Mn}_3(\text{PO}_4)_4 \cdot 2(\text{N}_4\text{C}_6\text{H}_{21}) \cdot 6(\text{H}_2\text{O})$

Mn-O2	2.02(1)	2×	Mn-O3	2.02(1)	2×
P1-O1	1.53(2)		P1-O2	1.49(1)	3×
P2-O3	1.53(1)	3×	P2-O4	1.57(2)	
O1-P1	1.53(2)		O2-Mn	2.02(1)	
O2-P1	1.49(1)		O3-Mn	2.02(1)	
O3-P2	1.53(1)		O4-P2	1.57(2)	
O4-Ow	2.71(1)	3×	Ow-O4	2.71(1)	
Ow-Ow	2.70(1)	2×			
N1-C1	1.49(1)	3×	C1-C2	1.52(1)	
N2-C2	1.48(1)				

Table 4. Selected Bond Angles [deg] for $\text{Mn}_3(\text{PO}_4)_4 \cdot 2(\text{N}_4\text{C}_6\text{H}_{21}) \cdot 6(\text{H}_2\text{O})$

O2-Mn-O2	104.9(8)		O2-Mn-O3	107.0(8)	2×
O2-Mn-O3	110.3(8)	2×	O3-Mn-O3	116.7(7)	
O1-P1-O2	104(1)	3×	O2-P1-O2	114(1)	3×
O3-P2-O3	107(1)	3×	O3-P2-O4	112(1)	3×
Mn-O2-P1	145.2(5)		Mn-O3-P2	123.9(6)	
C1-N1-C1	112(1)	3×	N1-C1-C2	113(1)	
C1-C2-N2	110(1)				

diffraction data and further evaluate the nature of the interlayer hydrogen bonding, molecular simulations of model manganese phosphate compounds were performed. Molecular simulation of these materials posed the challenge of adapting existing modeling approaches to new materials, especially those composed of both inorganic and organic components, thereby enhancing our understanding of the stability and behavior of these unique compounds.^{34–36}

Molecular models of the hydrous manganese phosphate TREN compound and an anhydrous version were created within the Cerius³⁷ molecular simulation software package. Periodic simulation cells were first created on the basis of the structure refinement results obtained from the powder diffraction data. The initial models were generated assuming a space group symmetry of $P\bar{3}c1$ but were then converted to $P1$ symmetry in order to provide full flexibility in the molecular mechanics simulations: no constraints on cell parameters and on atomic positions. We used the interatomic potentials of the Universal force field³⁸ which in our experience provides the

(32) Watkin, D. J.; Prout, C. K.; Carruthers, J. R.; Betteridge, P. W.; Cooper, R. I. *Crystals* Issue 11; Chemical Crystallography Laboratory, University of Oxford: Oxford, England, 2000.

(33) (a) Spek, A. L. *Acta Crystallogr., Sect. A* **1990**, *46*, C34. (b) Spek, A. L. *PLATON, A Multipurpose Crystallographic Tool*; Utrecht University: Utrecht, The Netherlands, 1998.

(34) Loiseau, T.; Mellot-Draznieks, C.; Sassoie, C.; Girard, S.; Guillou, N.; Huguenard, C.; Taulelle, F.; Ferey, G. *J. Am. Chem. Soc.* **2001**, *123*, 12744.

(35) Mellot-Draznieks, C.; Ferey, G. *Curr. Opin. Solid State Mater. Sci.* **2003**, *7*, 13.

(36) Cygan, R. T.; Kubicki, J. D.; Eds. *Molecular modeling theory: applications in the geosciences. Rev. Mineral. Geochem.* **2001**, *42*.

(37) *Cerius²-4.0 User Guide*, 4.2 ed.; Accelrys, Inc.: San Diego, CA, 1999.

most flexibility in modeling hybrid inorganic–organic materials. Nonetheless, selected force field parameters were modified to allow for the unique manganese coordination and bridging oxygens associated with the inorganic layer. The natural radius of the manganese was extended to 1.63 Å, and the natural angle was set to the idealized tetrahedral value of 109.47° to represent the four-coordinated environment of manganese; the Universal force field assumes by default an octahedral coordination for manganese. Additionally, the natural angles of the bridging oxygens for the manganese phosphate framework were altered to accommodate the variation observed in the crystallographic refinements. The natural angle associated with the Mn–O–P three-body interactions was set to 151° except for those associated with the P2 tetrahedra which were assigned a value of 125°. Otherwise, all other interatomic potentials, including those used to describe the organic TREN component, are taken directly from the Universal force field. Partial charges on all atoms were assigned on the basis of the charge equilibration³⁹ scheme and the geometry of the observed structure. The partial charges of the structural water molecules, however, were assigned manually in order to keep a uniform charge based on values obtained for a single gas-phase molecule.⁴⁰

Energy minimizations and molecular dynamics simulations were performed using the OFF energy program within Cerius.³⁷ Energy minimizations under constant pressure conditions were first performed for the anhydrous and hydrous models. The size of the simulation cell was based on the unit cell for each model. A spline cutoff method was used to evaluate the short-range van der Waals interactions, and an Ewald summation⁴¹ was used to calculate the long-range Coulombic interactions. The minimized configurations were used as the starting structures for the molecular dynamics simulations. The MD calculations were performed with both NVT (fixed cell parameters) and NPT (unconstrained cell parameters) canonical ensembles at 1 bar and 300 K using the Nose–Hoover⁴² and Parrinello–Rahman⁴³ methods to control temperature and pressure of the simulations, respectively. The Verlet⁴⁴ velocity algorithm was used to obtain accurate integrations and statistical ensembles using a time step of 0.001 ps. Equilibrium configurations and energies were typically obtained within 10–20 ps of the simulation. MD simulations were ultimately completed for times of 100 ps in length in order to ensure good statistical analysis of equilibrium structures; snapshot structures were saved every 50 time steps to provide a total of 2000 structures of the manganese phosphate TREN material.

The structural data for the energy-minimized structures are provided in Table 5 along with the observed experimental values. The energy-minimized structure for the hydrous phase, even though simulated under *P1* symmetry, provides symmetry corresponding to the *P3c1* space group to within a tolerance of 0.04 Å that is in agreement with the experimental structure. The same space group symmetry also is found to within 0.01 Å for the heavy elements of the structure after removal of the hydrogen atoms from the calculation. For the sake of comparison, the atomic coordinates of the structure of the hydrous compound, energy minimized with *P1* symmetry and then transformed to *P3c1*, are given Table 2 along with the experimental values obtained from the Rietveld refinement. All but the *c* parameter for both models have been accurately simulated with the present simulation method. We observe an approximate 15% expansion of the model values compared with the observed data. Note that only the basal

Table 5. Structural Data for Molecular Models Obtained from Energy Minimization

	energy minimized		experimental	
	anhydrous	hydrous	anhydrous	hydrous
<i>a</i> (Å)	9.068	9.030		8.8706
<i>b</i> (Å)	9.066	9.030		8.8706
<i>c</i> (Å)	25.129	30.33	22.8 ^a	26.158
α (deg)	89.97	90.00		90.
β (deg)	89.75	90.02		90.
γ (deg)	119.93	120.01		120.
<i>V</i> (Å ³)	1790.48	2141.73		1782.6
<i>D</i> (g/cm ³)	1.564	1.475		1.80

^a Determined from basal *d* spacing from X-ray diffraction and assuming same crystal system as hydrous phase.

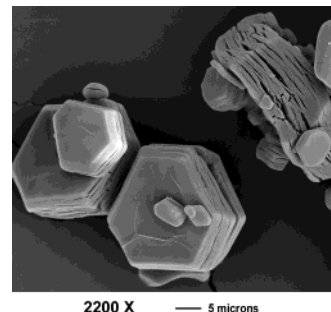


Figure 2. SEM micrograph of $\text{Mn}_3(\text{PO}_4)_4 \cdot 2(\text{N}_4\text{C}_6\text{H}_{21}) \cdot 6(\text{H}_2\text{O})$.

d-spacing was experimentally determined for the anhydrous material and that no absolute *c* value was obtained since the crystal system is at present unknown. Attempts to reduce this disagreement by increasing the net charge on the manganese phosphate layer and the TREN molecules failed; significant polyhedra distortions and loss of trigonal symmetry are observed. Similarly, the simulated volume and density are correspondingly about 15% too large and 20% too low, respectively. Nonetheless, the manganese phosphate layer and TREN molecules are remarkably accurate in comparison with the experimental structure (see Table 2). The four independent TREN molecules in the energy minimized model with *P1* symmetry have all the same conformation, equal to the one observed from the Rietveld structural refinement.

Results and Discussion

Physical Characterization. The pH of the synthesis solution was 11.5 and 10.8 before and after crystallization, respectively, and the product yield was 88% based upon total phosphorus. The resulting off-white powder is composed of stacked platelike crystals, as shown in Figure 2. The water-to-pyridine ratio could be varied from 1:0.4 to 1:44.2, at which point a large amount of amorphous impurity was observed. However, by substituting H_3PO_3 for the 85% H_3PO_4 , the hydrous manganese phosphate TREN compound could be obtained in pure pyridine without any amorphous impurity. When the molar amount of pyridine was less than that of water, small amounts of a crystalline impurity, believed to be $\text{NH}_4\text{MnPO}_4 \cdot \text{H}_2\text{O}$,²³ also formed.

The thermal analysis curve (shown in Figure 3) shows three distinct weight loss events: an 11.2 wt % loss by 200 °C; a 27.8 wt % loss between 250 and 500 °C; and an additional 10.2 wt % loss between 550 and 700 °C. The first event is attributed to the loss of interstitial water and agrees well with the calculated (11.4 wt %) water content. The second event corresponds to the decomposition of TREN and also agrees with calculated (30.9 wt %) values. The final weight loss event is

(38) Rappé, A. K.; Casewit, C. J.; Colwell, K. S.; Goddard, W. A.; Skiff, W. M. *J. Am. Chem. Soc.* **1992**, *114*, 10024.

(39) Rappé, A. K.; Goddard, W. A. *J. Phys. Chem.* **1991**, *95*, 3358.

(40) Berendsen, H. J. C.; Postma, J. P. M.; van Gunsteren, W. F.; Hermans, J. Interaction models for water in relation to protein hydration. In *Intermolecular Forces*; Pullman, B., Ed.; D. Reidel: Dordrecht, The Netherlands, 1981; p 331.

(41) Tosi, M. P. *Solid State Phys.* **1964**, *131*, 533.

(42) Hoover, W. G. *Phys. Rev. A* **1985**, *31*, 1695.

(43) Parrinello, M.; Rahman, A. *J. Appl. Phys.* **1981**, *52*, 7182.

(44) Verlet, L. *Phys. Rev.* **1967**, *159*, 98.

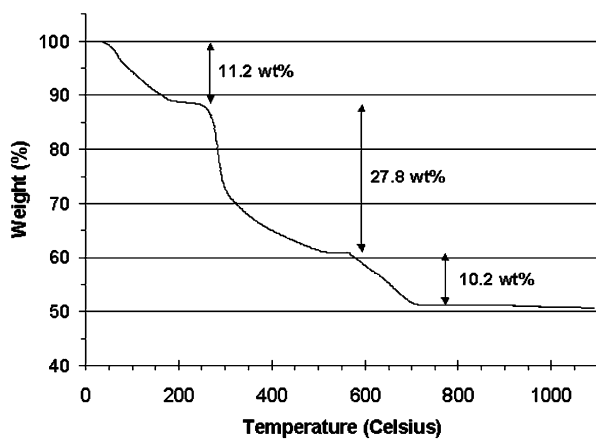


Figure 3. Thermogravimetric plot of $\text{Mn}_3(\text{PO}_4)_4 \cdot 2(\text{N}_4\text{C}_6\text{H}_{21}) \cdot 6(\text{H}_2\text{O})$.

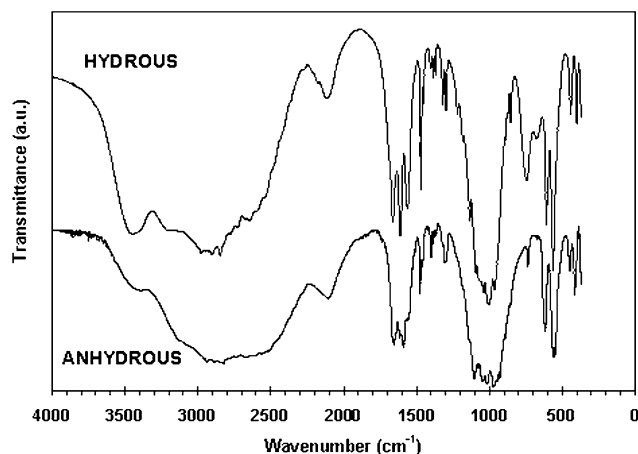


Figure 4. FTIR spectra of the hydrous and anhydrous TREN-MnPO phase.

attributed to loss of oxygen due to framework condensation, consistent with condensation behavior observed in other organically templated metal phosphate systems.⁴⁵ The product at 1000 °C is a glassy material that was not further investigated. The measured elemental composition of TREN-MnPO agrees very well with the composition derived from the structure determination (measured/calculated in wt %): Mn (17.2/17.3), P (12.8/13.0), O (37.0/37.0), N (11.8/11.8), C (15.3/15.1), H (6.0/5.7).

The infrared spectra of both hydrous and anhydrous TREN-MnPO are shown in Figure 4. Their complexity makes assignment of the individual absorption bands difficult, though the various regions can be ascribed as such:⁴⁶ the spectrum of the hydrous phase shows a strong band at 3450 cm^{-1} corresponding to the water molecules; the triplet between 1560 and 1660 cm^{-1} can be attributed to the ammonium groups bending modes. The stretching modes of the $-\text{CH}_2-$ groups of the TREN are in the 2500–3100 cm^{-1} domain whereas their bending modes range from 1200 to 1500 cm^{-1} . The intense and complex band centered at 1000 cm^{-1} and the sharp peaks at 563 and 609 cm^{-1} correspond to the modes of the PO_4 tetrahedra. The two broad peaks at

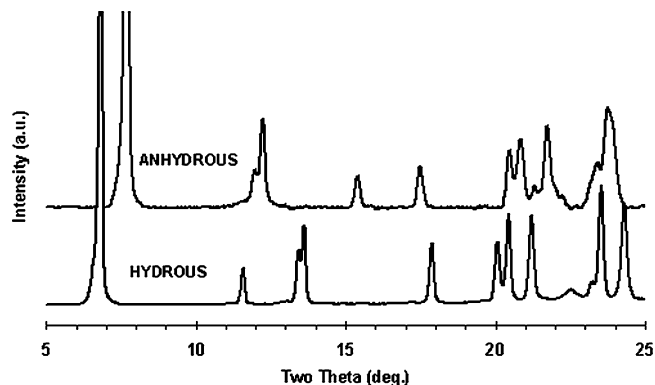


Figure 5. Powder X-ray diffraction pattern of the hydrous and anhydrous TREN-MnPO phase.

675 and 746 cm^{-1} are likely due to water librations.⁴⁷ The bands below 500 cm^{-1} can be ascribed to the Mn–O vibrations. The anhydrous compound exhibits essentially the same features, with a very marked reduction of the intensity of the water bands and an overall increase of the complexity of the pattern in the NH_3^+ and P–O regions compatible with the lowering in symmetry evidenced by its powder X-ray diffraction pattern (see Figure 5).

Determination of the luminescence spectrum of the inorganic framework was complicated by the strong spectral dominance of the TREN component. By measuring the spectrum of pure TREN and then subtracting it from the composite spectrum of the TREN-MnPO compound, the emission from the Mn(II) ion was ascribed to a broad peak centered at 560 nm. The complete lack of the characteristic 650 nm emission verifies that the manganese does not exist in an octahedral environment, and the shift to shorter wavelengths of the observed emission is suggestive of Mn(II) with tetrahedral coordination.⁴⁸

As verification that pyridine is not in any manner incorporated into the structure, the synthesis was performed using a complete (molar) substitution of ethylene glycol for pyridine. In this system, the hydrous manganese phosphate TREN compound was obtained at temperatures between 130 and 190 °C, by using water to ethylene glycol ratios that varied from 1:3 to 1:48. Minor amounts of crystalline $\text{NH}_4\text{MnPO}_4 \cdot \text{H}_2\text{O}$ ²³ occurred in these syntheses though in a nonsystematic fashion. Synthesis performed in pure water (no pyridine or ethylene glycol) at 170 °C yielded a mixture of $\text{Mn}_2(\text{PO}_4)\text{OH}$ ⁴⁹ and $\text{NH}_4\text{MnPO}_4 \cdot \text{H}_2\text{O}$,²³ indicating that TREN decomposes to ammonium groups under those conditions.

Structure Description. The inorganic layer, of composition $[\text{Mn}_3(\text{PO}_4)_4]$, is built-up by alternating corner-sharing MnO_4 and PO_4 tetrahedra (see Figure 6). The MnO_4 tetrahedron is fairly regular, with Mn–O distances of 2.02(1) Å and O–Mn–O angles ranging from 104.9(8)° to 116.7(7)°. The calculated bond valence sum⁵⁰ for the Mn site is thus 2.16, thereby confirming the Mn(II) assignment. In spinel type Mn_3O_4 (mineral Hausmannite), the Mn^{2+} site is also in a tetrahedral

(45) Bonhomme, F.; Thoma, S. G.; Nenoff, T. M. *J. Mater. Chem.* **2001**, *11*, 2559.

(46) Nakamoto K. *Infrared and Raman spectra of inorganic and coordination compounds*; John Wiley and Sons: New York, 1997.

(47) Tortet, L.; Gavarrri, J. R.; Nihoul, G.; Dianoux, A. J. *J. Solid State Chem.* **1997**, *132*, 6.

(48) Yen, W. M.; Ed. *Phosphor Handbook*; CRC Press: Boca Raton, FL, 1998.

(49) Waldrop, L. *Naturwissenschaften* **1968**, *55*, 296.

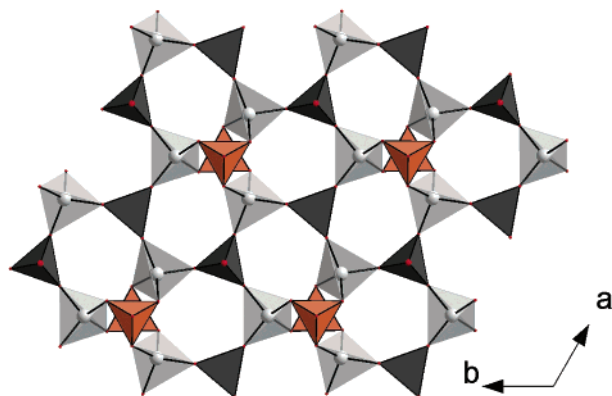


Figure 6. MnO_4 and PO_4 tetrahedra in $\text{Mn}_3(\text{PO}_4)_4 \cdot 2(\text{N}_4\text{C}_6\text{H}_{21}) \cdot 6(\text{H}_2\text{O})$: MnO_4 open, light gray; P1 dark gray; P2 light brown.

environment, with an average Mn–O distance of 2.01 Å.⁵¹ The MnO_4 group shares all its corners with the phosphate groups, whereas each phosphate tetrahedron contains one terminal oxygen atom, with the P–O bond pointing along the *c* axis. This leads to an uncondensed inorganic layer containing six- and four-membered rings. The O–O distances across the 6-ring opening are around 4.8 Å. The P2 atoms are located 2.14 Å above and below the mean plane of the layer that contains the Mn atoms (at $z = 1/4$ and $3/4$), whereas P1 is about 0.33 Å away from that plane.

The macroanion $[\text{Mn}_3(\text{PO}_4)_4]^{6-}$ resembles the aluminophosphate macroanion $[\text{Al}_3(\text{PO}_4)_4]^{3-}$ rather than other manganese phosphate macroanions due to the complete tetrahedral coordination of the metal atoms.^{52,53} The inorganic layer is a 4.6 net with ideal trigonal symmetry. The P1 tetrahedra belonging to the same 6-ring point in alternate directions, perpendicular to the layer, as illustrated in Figure 6. This up–down sequencing makes the inorganic layer of the title compound topologically most similar to that of *trans*-Co(dien)₂Al₃(PO₄)₄·3H₂O.⁵⁴

The negatively charged manganese phosphate layer $[\text{Mn}_3(\text{PO}_4)_4]^{6-}$ is sandwiched between two layers of triply protonated TREN molecules, with their ammonium groups pointing inward. The central nitrogen atom of the TREN (N1) is located on a 3-fold axis, directly above the apical P1–O1 bond. The terminal ammonium groups point toward the center of the 6-rings of the inorganic layer (see Figure 7). These neutral hybrid organic/inorganic layers are stacked along the *c* axis and separated from each other by a bilayer of water molecules (see Figure 8). Although the trigonal symmetry of the macroanion and the dimensions of the 6-rings and their separation are ideal for a template such as TREN, only one of the numerous $[\text{Al}_3(\text{PO}_4)_4]^{3-}$ type aluminophosphates, MIL-32, is templated by TREN.¹⁹ In MIL-32, however, the TREN molecules span the inorganic layers, rather than being hydrogen bonded to only one layer. Complete coverage of the surface of the layers by

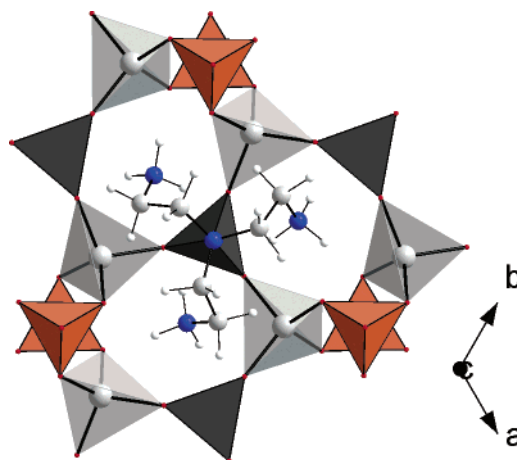


Figure 7. Location of TREN over the inorganic layer: MnO_4 open, light gray; P1 dark gray; P2 light brown. Nitrogen atoms of the TREN molecule shown in blue.

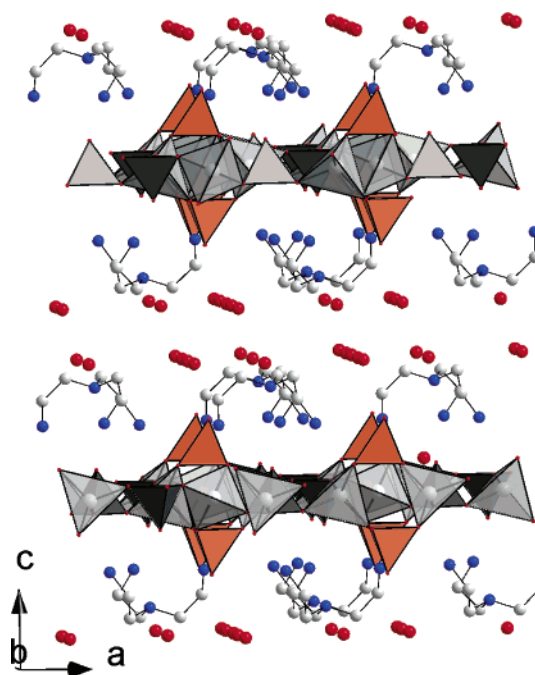


Figure 8. Layering of TREN, water, and inorganic sheets in $\text{Mn}_3(\text{PO}_4)_4 \cdot 2(\text{N}_4\text{C}_6\text{H}_{21}) \cdot 6(\text{H}_2\text{O})$: MnO_4 open, light gray; P1 dark gray; P2 light brown. Nitrogen atoms of the TREN molecule are blue; water oxygen atoms are large red. Hydrogen atoms omitted for clarity.

fully protonated TREN molecules can only be achieved with a macroanion of general formula $[\text{T}_3(\text{PO}_4)_4]^{6-}$, implying that T is a divalent metal in a tetrahedral environment.

The position of the hydrogen atoms of the water molecules cannot be uniquely determined by simple geometric consideration as was done for the TREN template; the discussion of the hydrogen bonding involving the water molecules is thus based on the results of the molecular modeling and the energy minimization procedure. The TREN molecules are hydrogen bonded to only one manganese phosphate layer. The minimum distance between the water molecules and the TREN ammonium groups is about 4 Å, indicating that there is no significant hydrogen bonding between the organic template and the water molecules. The bridging O2 and O3 atoms, part of the 6-ring, as well as the terminal

(50) Brown, I. D.; Altermatt, D. *Acta Crystallogr., Sect. B* **1985**, *41*, 244. (b) Brese, N. E.; O'Keefe, M. *Acta Crystallogr., Sect. B* **1991**, *47*, 192.

(51) Jarosch, D. *Miner. Petro.* **1987**, *37*, 15.

(52) Li, J.; Yu, J.; Yan, W.; Xu, Y.; Xu, W.; Qiu, S.; Xu, R. *Chem. Mater.* **1999**, *11*, 2600.

(53) Yu, J.; Xu, R.; Li, J. *Solid State Sci.* **2000**, *2*, 181.

(54) Bruce, D. A.; Wilkinson, A. P.; White, M. G.; Bertrand, J. A. *J. Solid State Chem.* **1996**, *125*, 228.

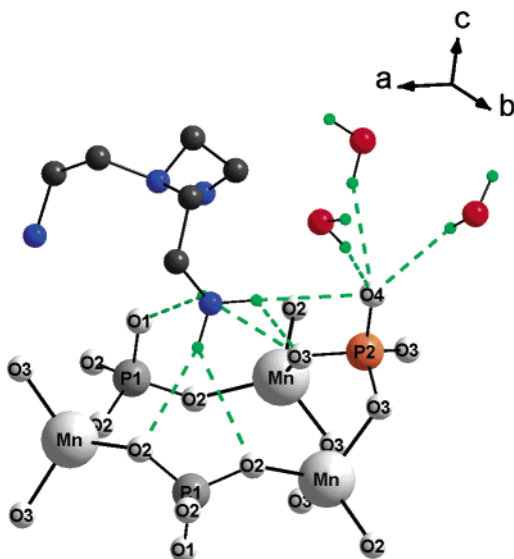


Figure 9. Hydrogen bonds between the inorganic layer and TREN (energy minimized structure): P2 atom light brown. Nitrogen atoms of the TREN molecule are blue; water oxygen atoms are red. Hydrogen atoms are green; carbon atoms are dark gray.

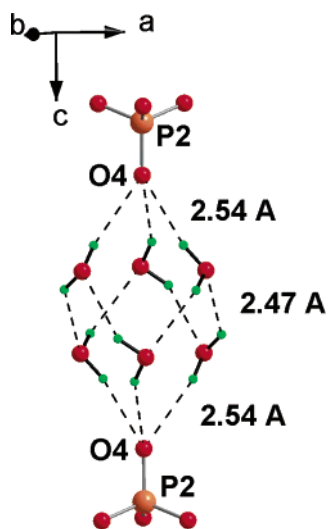


Figure 10. Hydrogen bonds between the inorganic layer and the water bilayer (energy minimized structure). Oxygen atoms are shown in red; hydrogen atoms are shown in green.

O1 and O4 atoms, hydrogen bond with the organic template (see Figure 9). It must be noted that Figure 9 depicts the energy minimized model but the same hydrogen bonding scheme is observed with the experimental structure derived from the Rietveld refinement and the geometrical placement of the H atoms of the TREN molecule. Each of the three ammonium groups of the template forms therefore 6 hydrogen bonds shorter than 3 Å with the $[\text{Mn}_3(\text{PO}_4)_4]^{6-}$ macroanion. The terminal O4 is also surrounded by three water molecules that are within hydrogen bonding distance, with $\text{O}-\text{H}\cdots\text{O}_4 = 2.54 \text{ \AA}$ (see Figure 10). These three water molecules, located in the same *ab* plane, do not however interact together. The energy minimized model of the hydrous material provides the stable configuration of a water bilayer, formed by clusters isolated from each other, each composed of six molecules forming a hydrogen bonded network having 3-fold axis of sym-

metry parallel to the *c*-axis. Hydrogen bonds distances ($\text{O}\cdots\text{H}$) between water molecules are around 2.47 Å and form a crownlike structure (see Figure 10). Significant insight into the disposition and behavior of the water bilayer was thus provided by molecular simulation. The interlayer stability is thus imparted mainly via hydrogen bonding between the inorganic layer and the bilayer network of hydrogen bonded water molecules. The MD models were helpful in evaluating the dynamic nature of the hydrogen bonding, although our MD simulations using within the canonical NPT ensemble failed to maintain a stable basal spacing for the structure, primarily due to the relatively low charges associated with the charge equilibration algorithm. However, MD simulations using the canonical NVT ensemble (i.e., with the lattice constants kept fixed at their experimental values) provide insight into the dynamical behavior of the hydrogen bonding associated with the hydrous compound. The water molecules reorient themselves while still maintaining the 3-fold symmetry for the oxygen atoms within the molecular water group. Additionally, hydrogen bonds (approximately 2.50 Å) form between the hydrogen atom of one of the cluster water molecules and the apical oxygen (O4) associated with the P2 phosphate groups. Similar hydrogen bonding (approximately 2.29 Å) exists between the amine hydrogens of the TREN molecules and the apical oxygen (O1) of the P1 phosphate groups. Although transient in occurrence (on the order of hundreds of femtoseconds) the hydrogen bonds constitute a dynamic stabilizing effect on the entire structure.

The bilayer of water is fairly labile, and the compound can undergo a complete reversible dehydration, as shown by TGA and subsequent X-ray diffraction experiments. The sample was maintained in the TGA at 175 °C under flowing air for 3 h, reaching a weight loss at equilibrium of 11.0% attributable to the quasicomplete loss of water (expected loss of 11.4%). The quenched anhydrous sample was then rapidly transferred to the X-ray diffractometer and measured in air (relative humidity ~ 35%) at room temperature. The powder pattern for the anhydrous phase showed a decrease in the interlayer spacing of the main peak (002 for the hydrous phase) from 13.1 to 11.4 Å (see Figure 5). Successive diffraction patterns showed a gradual rehydration, without loss of crystallinity, which was complete after approximately 1 h. No phase with intermediate interlayer spacing was observed, indicating that the rehydration likely proceeds in one step, directly from the anhydrous to the fully hydrous state. Under dryer conditions (relative humidity < 15%), a similarly dehydrated sample remained stable at room temperature for more than 24 h. However, the sample could be fully rehydrated after being exposed for 1 min to water-saturated air at 65 °C. The powder diffraction pattern of this stable anhydrous sample could not be indexed by a similar trigonal cell with a shorter *c* axis, indicating a probable lowering in symmetry likely due to a small displacement of the layers with respect of each other. The presumably lower symmetry of the anhydrous sample and its poor crystallinity have so far thwarted our attempts at *ab initio* indexation. A sample maintained for a week in air at 175 °C showed the same powder pattern and rehydration behavior, indicating

that the phase is very stable under those conditions and thus no template loss or decomposition occurs. Only a few other examples of reversible dehydration in metal phosphates have been reported.^{55–57}

Conclusion

A novel layered TREN-templated manganese(II) phosphate compound, $\text{Mn}_3(\text{PO}_4)_4 \cdot 2(\text{N}_4\text{C}_6\text{H}_{21}) \cdot 6(\text{H}_2\text{O})$, has been synthesized. This compound differs from other layered manganese phosphate compounds in that all of the manganese is tetrahedrally coordinated; the $[\text{Mn}_3(\text{PO}_4)_4]^{6-}$ macroanion most closely resembles the aluminophosphate macroanion $[\text{Al}_3(\text{PO}_4)_4]^{3-}$. Furthermore, contrary to what is generally observed for other layered organic–inorganic metal phosphates, the or-

ganic in the present compound does not contribute to interlayer stability; its primary role is charge balancing for the inorganic macroanion. Structural stability is provided via a network of hydrogen bonds between water molecules and the inorganic layer. Synergistic modeling combining ab initio structure determination from powder X-ray diffraction data with molecular simulation methods has helped identify and characterize the structure and bonding behavior of this unique hybrid material.

Acknowledgment. The authors would like to thank Dr. B. L. Abrams for photoluminescence measurements. This research (RTC) was supported in part by the U.S. Department of Energy, Office of Basic Energy Sciences, Geosciences Research. Sandia is a multiprogram laboratory operated by Sandia Corporation, a Lockheed Martin Company for the U.S. Department of Energy under Contract DE-AC04-94AL85000.

(55) Natarajan, S.; Eswaramoorthy, M.; Cheetham, A. K.; Rao, C. N. R. *Chem. Commun.* **1998**, 15, 1561.

(56) Thomas, J. M.; Jones, R. H.; Xu, R.; Chen, J.; Chippindale, A. M.; Natarajan, S.; Cheetham, A. K. *J. Chem. Soc., Chem. Commun.* **1992**, 929.

(57) Choudhary, A.; Natarajan, S.; Rao, C. N. R. *Chem. Mater.* **1999**, 11, 2316.

CM0348444